GERDA

Progress report to the LNGS scientific committee

(Appendix)

LNGS-EXP 33/05 add. 6/08

The format of this GERDA progress report differs from our earlier ones to facilitate both fast and in-depth reading. A *short write-up* (`http://www.mpi-hd.mpg.de/GERDA/reportsLNGS/gerda-lngsSC-shwup-apr08.pdf`) summarizes concisely the achievements during the last six months and highlights important issues. An *appendix* to the report (`http://www.mpi-hd.mpg.de/GERDA/reportsLNGS/gerda-lngsSC-appdx-apr08.pdf`) provides additional technical and experimental details for follow-up reading.

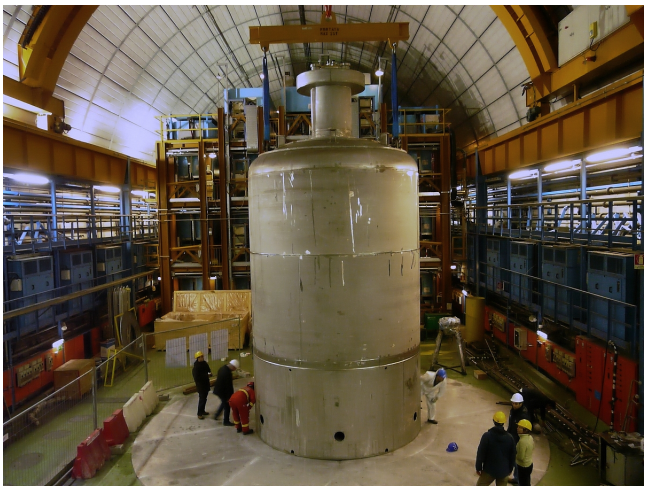

April 2008

A.M. Bakalyarov [h], M. Balata [a], I. Barabanov [f], L. Baudis [m], C. Bauer [c], E. Bellotti [e], S. Belogurov [f,g], S. T. Belyaev [h], M. Barnabe-Heider [c], A. Bettini [j], L. Bezrukov [f], V. Brudanin [b], R. Brugnera [j], D. Budjas [c], A. Caldwell [i], C. Cattadori [a,e], O. Chkvorets [c], E. V. Demidova [g], A. Di Vacri [a], A. D'Androgora [a], V. Egorov [b], A. Ferella [m], F. Froborg [m], N. Fodyma [d], A. Garfagnini [j], A. Gangapshev [f], J. Gasparro [l], S. Gazzana [c], P. Grabmayr [k], G. Y. Grigoriev [h], K. N. Gusev [h], V. Gurentsov [f], W. Hampel [c], M. Heisel [c], G. Heusser [c], W. Hofmann [c], M. Hult [l], L.V. Inzhechik [h], J. Janicsko [i], M. Jelen [i], J. Jochum [k], M. Junker [a], S. Katulina [b], J. Kiko [c], I.V. Kirpichnikov [g], A. Klimenko [b,f], M. Knapp [k], K.T. Knoepfle [c], O. Kochetov [b], V.N. Kornoukhov [f,g], K. Kroeninger [i], V. Kusminov [f], M. Laubenstein [a,e], V.I. Lebedev [h], D. Lenz [i], M. Lindner [c], J. Liu [i], X. Liu [i], B. Majorovits [i], G. Marissens [l], I. Nemchenok [b], L. Niedermeier [k], J. Oehm [c], L. Pandola [a], K. Pelczar [d], P. Peiffer [c], A. Pullia [e], F. Ritter [k], C. Rossi Alvarez [j], V. Sandukovsky [b], S. Schoenert [c], J. Schreiner [c], J. Schubert [i], U. Schwan [c], B. Schwingenheuer [c], M. Shirchenko [h], H. Simgen [c], N. Smale [c], A. Smolnikov [b,f], F. Stelzer [i], L. Stanco [j], A.V. Tikhomirov [h], U. Trunk [c], C.A. Ur [j], A.A. Vasenko [g], S.Vasiliev [b,f], M. Wojcik [d], E. Yanovich [f], J. Yurkowski [b], S.V. Zhukov [h], E. Zocca [e], G. Zuzel [c]

[a] INFN Laboratori Nazionali del Gran Sasso, Assergi, Italy
[b] Joint Institute for Nuclear Research, Dubna, Russia
[c] Max-Planck-Institut für Kernphysik, Heidelberg, Germany
[d] Institute of Physics, Jagellonian University, Cracow, Poland
[e] Università di Milano Bicocca e INFN Milano, Milano, Italy
[f] Institute for Nuclear Research of the Russian Academy of Sciences, Moscow, Russia
[g] Institute for Theoretical and Experimental Physics, Moscow, Russia
[h] Russian Research Center Kurchatov Institute, Moscow, Russia
[i] Max-Planck-Institut für Physik, München, Germany
[j] Dipartimento di Fisica dell'Università di Padova e INFN Padova, Padova, Italy
[k] Physikalisches Institut, Universität Tübingen, Germany
[l] Institute for Reference Materials and Measurements, Geel, Belgium
[m] Physik Institut der Universität Zürich, Zürich, Switzerland

Spokesperson: S. Schönert,
(Stefan.Schoenert@mpi-hd.mpg.de)
Co-Spokesperson: C. Cattadori
(Carla.Cattadori@lngs.infn.it)
Technical Coordinator: K.T. Knöpfle
(Karl-Tasso.Knoepfle@mpi-hd.mpg.de)

URL: http://www.mpi-hd.mpg.de/GERDA/reportsLNGS/gerda-lngsSC-appdx-apr08.pdf

Contents

1 Phase I detectors

In total 17.9 kg of enriched and 15 kg of non-enriched high-purity germanium detectors, which were used in the past in the HdM and Igex experiments and in the Genius Test Facility (GTF), will be operated in Phase I of Gerda. As described in earlier reports, the preparation of Phase I detectors has been broken down into five distinct work packages (WP). The main activities during the last six months concerned WP3 (testing of Phase I prototype detector assemblies) with emphasis on the study of gamma radiation induced leakage currents (LC), and WP5 (construction of the low-background test stand LArGe) including studies for background identification by pulse shape analysis of LAr scintillation. The completion of WP4 (processing of enriched and non-enriched detectors) is pending upon the results of WP3.

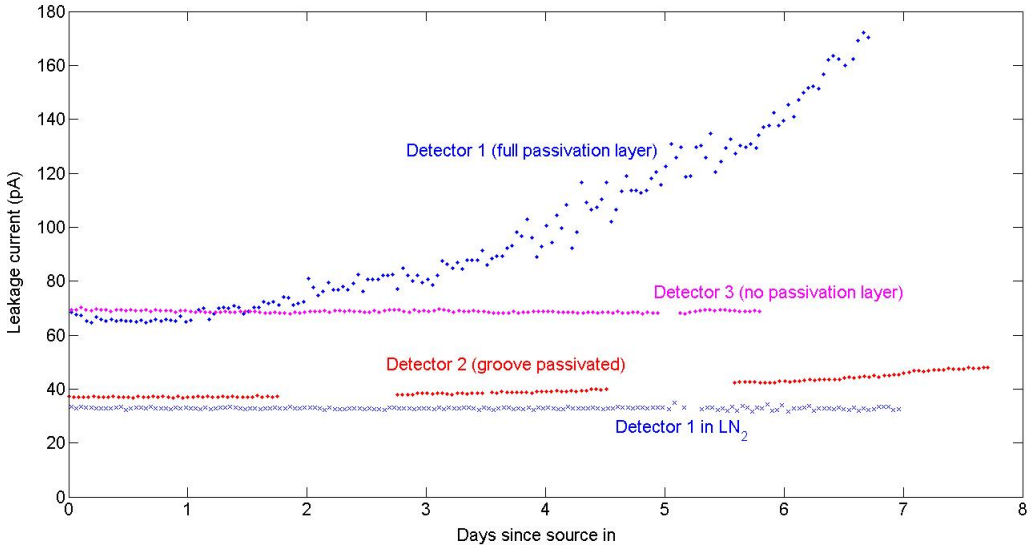

Figure 1: Comparison of leakage current changes under gamma irradiation for three detectors with different passivation layer configurations operated in liquid argon. Reducing the size of the passivation layer to the groove area (detector 2/GTF-42) strongly reduces the increase of LC under gamma radiation. No LC increase is observed for the detector without passivation layer in LAr (detector 3/GTF-44) and similar, for detector 1 in liquid nitrogen. All leakage current increases were found to be fully reversible.

1.1 Gamma radiation induced leakage current

Operations with Phase I prototype detector assemblies continued in the Underground Detector Laboratory (Gdl) at Lngs. A second test stand for long-term measurements and irradiation tests is now operational. Thus two prototype detectors can be operated simultaneously. Two additional non-enriched crystals (GTF-42 and GTF-44) with modified

passivation layer geometries have been prepared in October 2007 by Canberra, Olen in order to study its impact on the gamma induced LC. In total, there are now three Phase I prototype detectors under investigation with different passivation layer geometries. The passivation layer of the first prototype detector (GS935) covers quasi the full front face of the crystal. For the crystal GTF-42 it has been limited to the area of the groove while for GTF-44 no passivation layer has been applied. The measured energy resolution of the GTF-42 using standard FE electronics with about 1 m cables between crystal and FET is 3.0 keV (FWHM) at 1.3 MeV.

Fig. 1 shows the increase of LC under identical gamma radiation and bias voltage conditions for the different detector configurations. A 44 kBq ^{60}Co is located at approximately 20 cm distance irradiating mainly the signal contact side. The experimental observation that the reduction in area of the passivation layer reduces the LC increase under gamma radiation, corroborates our hypothesis that charge collection on the surface of the insulating passivation layer is the origin of the (reversible) LC increase. Moreover, no radiation induced LC increase has been observed when operating GS935 in liquid nitrogen.

The measurements with GTF-42 and GTF-44 in LAr are ongoing and the LC values are stable at 10 pA and 5 pA respectively. A periodic 10 minutes irradiation of GTF-42 with a ^{60}Co gamma source is carried out once per week in order to simulate the energy calibration in GERDA, while monitoring the leakage curent stability with high accuracy.

1.2 Processing of Phase I detectors

Based on the results summarized in the previous section, it is planned to implement a passivation layer which is limited to the groove area only. Despite the fact that the crystal without passivation layer shows the best behavior with respect to LC increase under gamma irradiation, it is less favored for technical and handling reasons. The time period to complete the detector processing is under discussion with the manufacturer. In the mean time the crystals are stored underground to avoid cosmogenic activations.

1.3 Low-background test stand LARGE

The assembly of the cryostat was carried out at the manufacturer and the inner vessel with the integrated heat-exchanger and thermal shield was delivered to MPIK. Despite an earlier successful He-leak test, the heat exchanger showed leaks at the weld joining the heat-exchanger and the thermal shield. The vessels were returned to the manufacturer and extensive repair work carried out. Helium leak tests were carried after completion of the repair work prior and after the first liquid nitrogen cooling of the heat-exchanger, thermal shield and inner vessel (Fig. 2). The inner vessel assembly returned to MPIK in the last February week to complete the mounting of the IR-reflection shields and of the outer vessel. The cryostat will be installed in the GDL after completion of the cryogenic tests.

Figure 2: Left: Mounting of the thermal shield of the LArGe cryostat. Right: first cool-down of the integrated heat-exchanger after completion of the welding to the inner vessel and thermal shield.

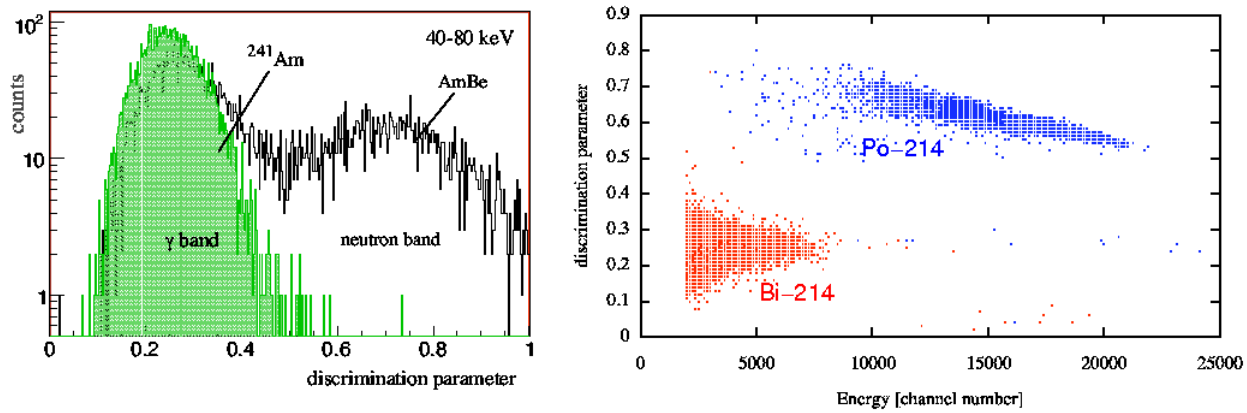

Figure 3: Left: Distribution of the LAr scintillation pulse shape discrimination parameter in an energy range of 40 keV to 80 keV from an internal ^{241}Am gamma source and from an external AmBe neutron/gamma source. Right: Scatter plot with alpha (blue) and gamma (red) events from ^{214}Bi–^{214}Po decays.

1.4 Background identification by pulse shape analysis of LAr scintillation

Laboratory work on background identification using the pulse shape of liquid argon scintillation has been further pursued. Fig. 3 displays the pulse shape discrimination parameter for low-energy gamma and neutron interactions (left canvas) and high-energy beta/gamma and alpha energy depositions (right canvas). In the framework of the R&D of instrumenting the liquid argon, it is planned not only to use the liquid argon scintillation light as a veto signal, but to exploit the pulse shape information of the liquid argon scintillation signal to identify the origin of background events. Examples are the identification and discrimination of radon decays in the liquid argon using the BiPo-214 time correlation together with the pulse shape information, and of the ^{77}Ge production and decay using the pulse shape of the neutron–argon scattering followed by the prompt gammas of the neutron capture in ^{76}Ge.

2 Phase II detectors

2.1 Prototype testing

Since the last report the construction of the prototype of the cryostat which will be used for crystal tests in the GERDA cleanroom was finished. It was installed in a clean room at the MPI in Munich and became operational (Gerdalinchen II, c.f. Fig.4). At the moment of writing we are running tests with germanium detectors and soon an 18 fold segmented prototype detector will be tested. The new cryostat can hold up to three crystals, has an infrared shield and offers better control of temperature and humidity during cool-down and warm-up cycles. With the possibility to introduce a radioactive source inside the cryostat, we will be able to measure the properties of our detector with better spatial resolution.

2.2 Production of Phase II detectors

After the first successful test of the purification of GeO_2 at PPM Pure Metal, reported in the previous Progress Report, a second test was performed. The goal of the second test was to increase the yield of the 6N material and to define a procedure for minimizing cosmic exposure. No mass spectrometry measurements were done at this time.

As in the previous test, the depleted GeO_2 (<1 % ^{76}Ge) is reduced to metallic Ge in a reduction furnace, and then zone refined. After zone refinement a resistivity measurement is performed. The part of the ingot with less than 50 Ωcm is cut off and reprocessed. In the first test, after two iterations of zone-refinement a yield of 77% was achieved. This time after three runs of zone-refinement the total yield achieved was around 90%. This excellent result means that most of the enriched material can be used to pull crystals.

The second goal of the test was to reduce the exposure of the germanium to the cosmic radiation. The material was temporarily stored underground in a nearby mining museum.

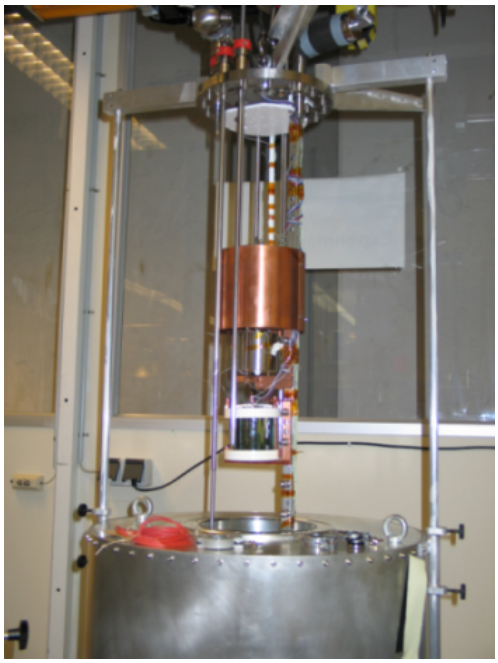

Figure 4: A germanium detector being lowered in the test cryostat

The test proved that transporting the material back and forth to the underground storage is feasible and the time above ground for the purification should not exceed two-three days.

2.3 Crystal characterization

It is forseen to pull the crystals necessary for Ge detectors at the Institut für Kristallzüchtung (IKZ) in Berlin. Producing detector grade material is not possible without the adequate measurement techniques. In order to measure such a low level of impurities, IKZ set up a Hall-effect measurement and a PTIS (Photo-Thermal Ionization Spectroscopy) setup. The first tests are already completed. In Fig. 5 we can see the net concentration of the charge carriers versus 1/T. The measurement is done down to 15 K on a sample crystal purchased by MPI from Canberra for this particular purpose. We can clearly see the transition from intrinsic conductivity to extrinsic. After the freeze-out of the intrinsic charge carriers, the net concentration of charge carriers is in the order of magnitude of $10^{10}/cm^3$. This is the purity level that should be achieved in the crystals in order to produce large detectors.

In order to continuously monitor the purity of the material, pulling small test crystals will be regularly needed. IKZ already pulled a small crystal from the zone-refined material produced during the first purification test at PPM. The first (preliminary) Hall-effect measurement suggest that the concentration of impurities in the zone-refined material is between 10^{12} and $10^{11}/cm^3$. This numbers are consistent with the one deduced from resistivity measurement mentioned in the previous Progress Report and they are far better than expected, since this Ge is rated as 6N material.

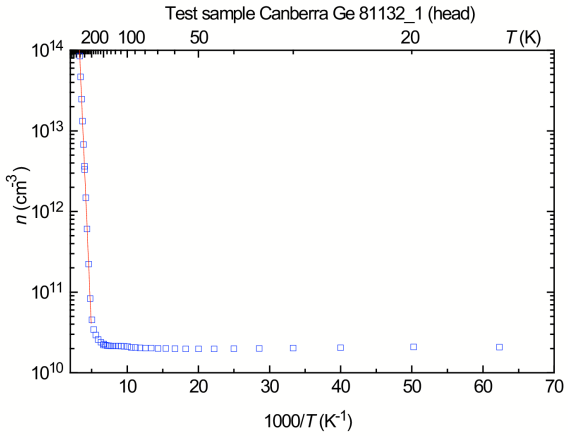

Figure 5: Hall-effect measurement of charge carrier concentration on a detector grade germanium crystal.

Another important measurement technique is the Photo-Thermal Ionization Spectroscopy. This is a qualitative method that reveals the chemical composition of the impurities present in the crystal. It is complementary to the Hall-effect measurement, which is a quantitative test. IKZ completed their setup based on a standard Fourier transform infrared spectrometer. They proved the correct functioning with a Si sample and they already measured the Canberra sample crystal. The spectra can be seen in Fig. 6.

First crystals from a dedicated Czochralski puller will be produced in March 2008 and analyzed to determine whether further purification at PPM is necessary. First detector grade crystals are expected by the end of the year.

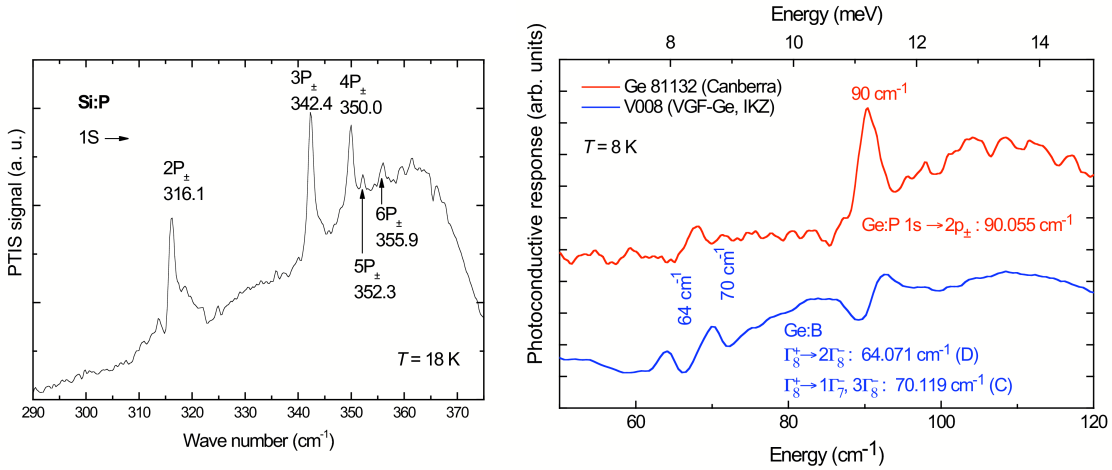

Figure 6: PTIS spectrum of silicon(left) and detector grade germanium (right)

2.4 Status of the Czochralski puller

Refurbishing of the Czochralski puller was finished recently. In order to reduce the contamination from the equipment, copper parts were removed and replaced with silver, the graphite susceptor crucible was replaced with molybdenum and all internal parts are supported by high purity quartz holders. High purity quartz crucibles are being purchased to hold the germanium melt. The puller is already set up to produce 2“ crystals, and larger crystals will be made once the larger crucible is available. First crystals pulled of natural (6N) germanium are expected at the time of writing.

3 Cryogenic vessel and infrastructure

On 6 March 2008, the cryostat was delivered to LNGS and placed at the foreseen location in Hall A. Compared to its 'quasi-final' schedule, Rev. 5 of 21 September 2007, the delivery was delayed by 3 weeks.[1] The commissioning of the cryostat in Hall A is proceeding faster than originally scheduled (see below) so that the water tank construction is expected to start in the week of 21 April. This corresponds to a delay of 3 months with respect to the GERDA schedule presented in April 2007.

Table 1 provides a chronological list of some final acceptance tests of the cryostat. The pressure tests for the inner and outer vessel under the inspection of TÜV have been the final tests according to the German pressure vessel code AD2000. Once the documentation is finalized and checked both vessels will receive CE certificates according to PED 97/23/EC.

The helium leak tests yielded the requested vacuum performance. Also the pump-down time for the insulation vacuum of about 2 weeks turned out to be fully acceptable; this is gratifying since the inner vessel carries not only the multi layer insulation but also in its cylindrical part a 6 mm thick Makrolon layer as additional passive insulation in case of leakage of the outer vessel (Fig. 7).

The inner vessel rests on 8 support pads. To ensure that all pads carry equal load when the cryostat is filled, a non-standard test (Fig. 8) was carried out: when the (empty) inner vessel was inserted into the outer one, load cells measured the weight on each of the pads. Since each pad rests on a Belleville spring with known spring constant the differences between the loads can be transformed to length differences of less than 0.1 mm. Thus all pads will carry about equal load once the cryostat is filled.

The evaporation test (Fig. 9) showed that the heat input to the cryostat is lower than specified.

The Rn emanation rate of the cryostat is a crucial value since Monte Carlo studies indicate that a homogeneous distribution of 8 mBq of ^{222}Rn would add 10^{-4} cts/(keV·kg·y) to the background index.[2] Two measurements after a first cleaning cycle of pickling,

[1] The cryostat could have been delivered almost in-time if the final pressure test of the outer vessel had taken place as scheduled. Due to a discrepancy between an actual weld and its specification in the weld map this test was canceled twice.

[2] Anti-coincidences between diodes and/or segments are not taken into account in this number. If these are applied for the phase II setup then the allowed activity is 14 mBq for a background index of

Figure 7: Mounting of the Makrolon sheets onto the outer surface of the inner vessel (left), and insertion of the inner vessel (covered by the multilayer insulation) into the outer vessel.

passivation and rinsing with de-ionized water yielded values which differed by almost a factor of two: 16.9 ± 1.6 mBq for the first and 29.8 ± 2.4 mBq for the second extraction. A possible explanation is a fractioning of Rn inside the cryostat: the heavier radon is concentrated at the bottom. Due to the measurement procedure the radon concentration is then enhanced in the second sample. A visual inspection showed that the inner surface was not metallic bright after the first cleaning. Thus, mechanical grinding of areas with e.g. tape remnants and another cleaning cycle was done. The efficiency of this cycle was reduced due to a low steel temperature of 2 °C.

The subsequent emanation measurement at LNGS yielded two consistent values with an average of 13.7 ± 1.9 mBq. In this case, the gas inside the cryostat was mixed before the samples were extracted. Scaled for the cryostat's size these results compare favorably with values measured for other vessels. Thus, without another cleaning cycle, the installation of the internal copper shield started. Further tests scheduled after Easter are a He leak test and another evaporation test in order to verify that the cryostat has not been damaged during transportation. Afterwards another emanation test will take place and its outcome will influence the final cleaning procedure.

The cryostat's cryogenic infrastructure has been tendered European wide based on

10^{-4} cts/(keV·kg·y).

Table 1: List of some of the recent activities and of the acceptance tests the cryostat has passed. Tests until February 27 have been done at the manufacturer SIMIC, the test at March 11 after delivery to Hall A of LNGS.

Date	test	specification / result
12 Nov 07	pressure test of inner vessel	3.6 barg water
26 Nov 07	He leak test of inner vessel	$< 5 \cdot 10^{-9}$ mbar ℓ / s
05 Dec 07	Rn-222 emanation test, 1st extraction (23 m^3)	17 mBq
06 Dec 07	Rn-222 emanation test, 2nd extraction (30 m^3)	30 mBq
12 Dec 07	load test of support pads of inner vessel	passed
15 Jan 08	He leak test of outer vessel	$< 10^{-7}$ mbar ℓ / s
28 Jan 08	LN2 evaporation test of completely filled	$<$ 4 Nm^3/h, or $<$ 300 W
04 Feb 08	2nd pickling & passivation cycle of inner vessel	at (low) 2 °C
27 Feb 08	pressure test of outer vessel	1.85 barg N2
11 Mar 08	Rn-222 emanation test, 2 extractions (44/40 m^3)	13.6/13.7 mBq
18 Mar 08	internal copper shield installed	

detailed technical specifications. The respective TED document 2008-27384 was published on 31 January 2008 and the time limit for submission was 17 March. Unfortunately, we received no adequate offer. Negotiations with some selected companies have started.

The last item to be tendered is the heater for the Ar exhaust gas. The final decision on its dimension and type is pending.

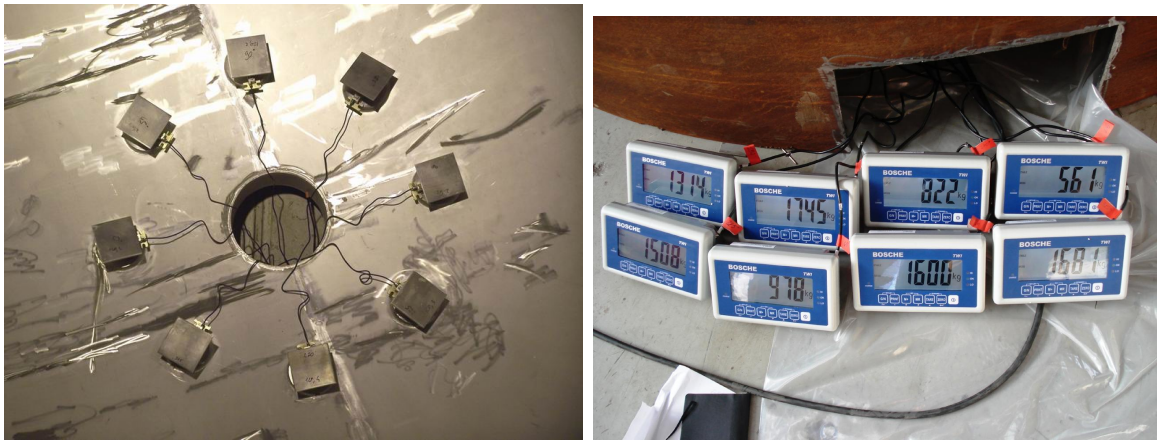

Figure 8: The 8 load cells arranged on the support pads at the bottom of the outer vessel (left), and the measured loads (in kg) on the individual pads after the inner vessel has been lowered onto the pads. The stiffness of the Belleville spring below each pad is 59 kN / mm.

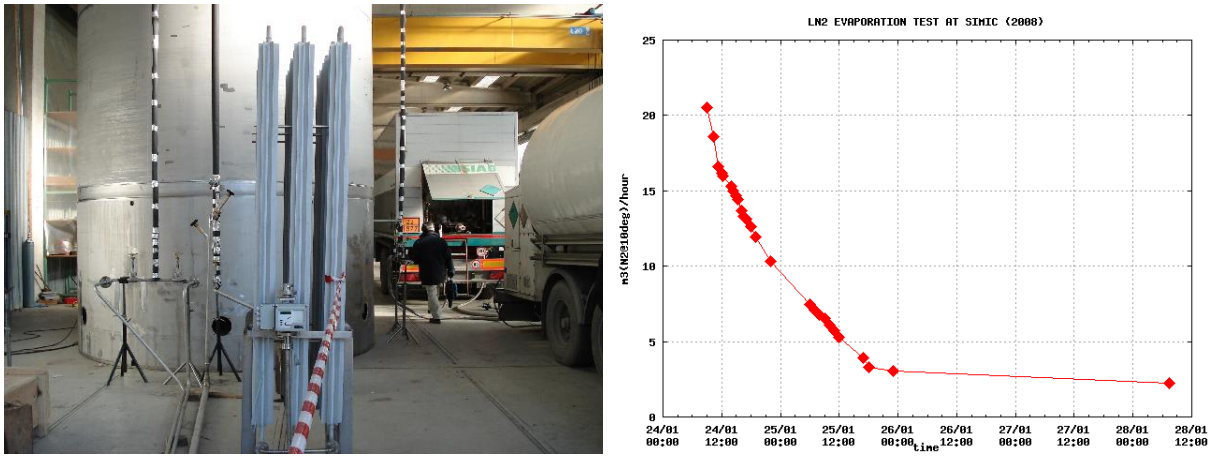

Figure 9: Set up for the evaporation test at SIMIC (left), and the measured evaporation rate during the settling time of the cryostat after being completely filled with liquid nitrogen.

4 Water tank and water drainage

The steel of the water tank (WT), the flanges, PMs anchorages etc., are all available at the company site, waiting to be mounted at LNGS around the cryogenic vessel (week 17). The company charged with the WT installation has provided to the collaboration and to LNGS SPP the detailed plans for the construction procedures, which have been reviewed and approved by the latter. The WT mounting procedure is illustrated by Fig. 10. A circular corona of the roof will be put together at floor level, then lifted up and the first ring of the WT mantle will be welded (2 m height), then everything will be lifted up, the second ring will be mounted at floor level, then welded at the first one, then lifted up and so on. Finally the inner part of the WT roof will be welded to the roof circular corona.

A fast drainage of the water is needed in case of serious lost of thermal insulation of the cryostat. Discharging proceeds via two pipes. One DN250 pipe was put below the TIR tunnel during the recent civil works. It has a maximum flow rate 56 l/s of which 46 l/s are available for GERDA. A second DN150 pipe with 16 l/s leads to the Hall A pits which are devoted to collect any fluid accidentally discharged by experimental activities. Finally, as *ultima ratio*, water will be discharged also on the floor of the TIR tunnel in case of emergency. All options should allow to drain the complete water (650 m^3) within 2 hours. Details of the water discharging procedures are not yet completely defined and approved by the LNGS technical staff. Moreover, procedures and hardware to discharge the water are also related to the cryogenic gas heater type and dimension; the latter has not yet been accepted/defined by LNGS.

The pure water will be produced by the Borexino water plant. It will be recirculated by a closed circuit equipped with an Ultra-Q unit to keep the water clean for Cerenkov light detection.

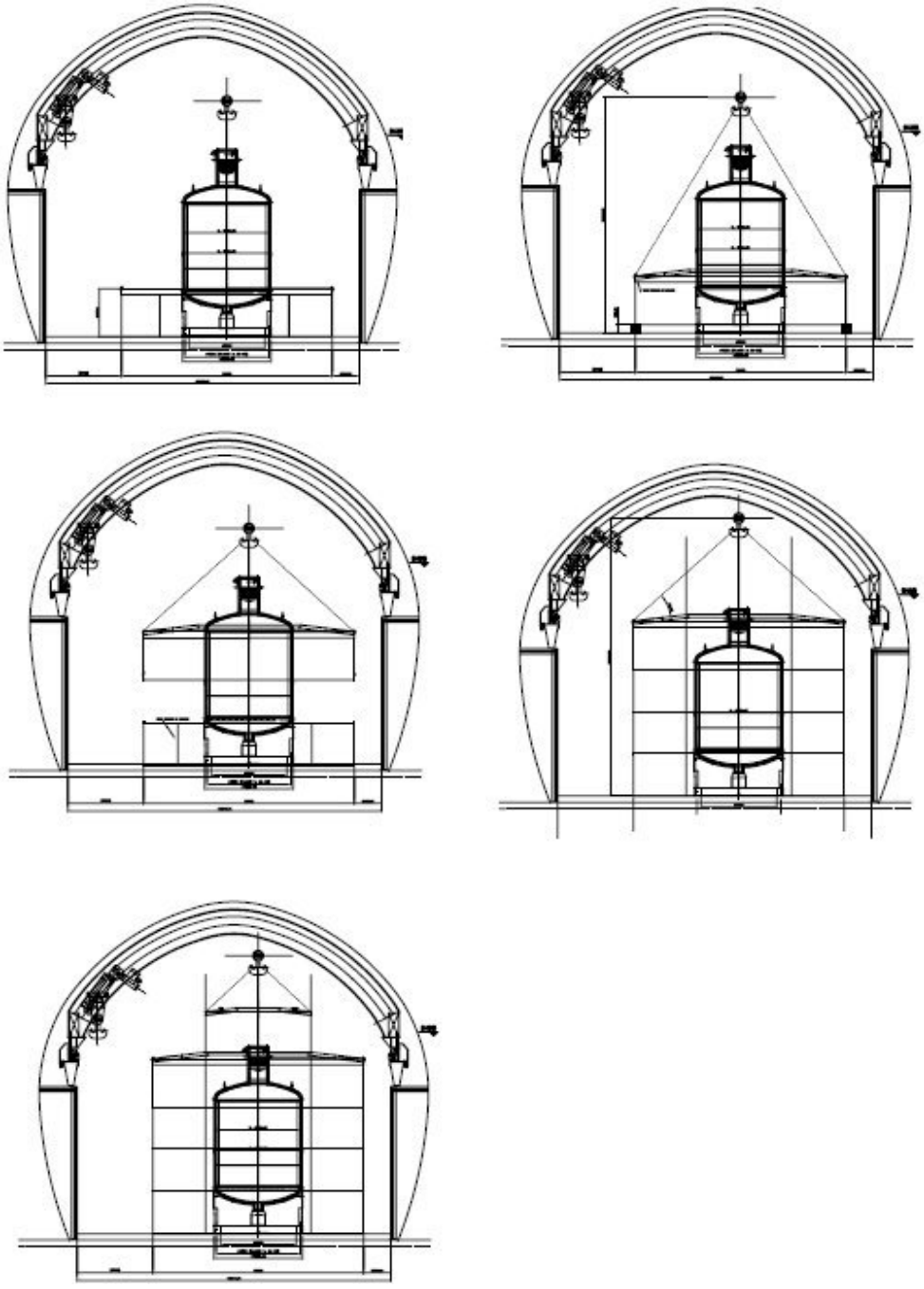

Figure 10: The WT mounting procedure.

5 Clean Room and Lock System

5.1 The Clean Room

Detectors will be prepared for installation into the cryostat inside the clean room. Strings with three detectors will be preinstalled underneath flow boxes of class 100 before they are inserted to the lock system.

The design of the clean room is finished. The technical specifications are defined in a tendering document. Fig. 11 shows a 3D model of the clean room.

The limited invitation to tender has been closed and three companies are identified. The contract with the winning company is scheduled to be signed by calendar week 20. The installation of the clean room could start beginning of October 2008.

5.2 The Lock system

The strings with the detectors will be lowered to the cryostat through the lock system. Boundary conditions require the lock to be a vacuum tight pressure vessel. It will be produced out of stainless steel. The lock cylinder will rest on a support structure that is bolted to the HEB700 superstructure beams resting on damping feet which decouple the lock from high frequency vibrations of the superstructure. Strings with up to five detectors can be inserted to their final array position within the cylinder by a rail system. A linear pulley system lowers the detector strings to the cryostat.

The design of the complete lock structure is almost finished. Production of the first components has commenced. The complete lock system will be preinstalled at the MPI in Munich in the course of 2008. The transport of the fully installed system is scheduled for early 2009.

The PLC system for control of the motors running the linear pulleys has been designed and is currently being equipped and tested at the MPI in Munich.

5.3 The Cable Tree

The cable guide on which the strings are lowered and the cables and string contact matrix connecting the detectors to the power supply and the DAQ outside the lock have been defined in cooperation with TG3 for phase I. They are already in production. Electrical tests have been carried out with a full phase I cable tree inside liquid nitrogen and including the connecting matrix using HPGe detectors. It could be demonstrated that no significant deterioration of the pulses occur and that cross talk is tolerable ($\leq$3 per mill). The energy resolution of a HPGe detector with 2.2 keV at 1460 keV was shown to be unaltered by connecting the cable tree between preamplifier and DAQ system. Thus an increase of the FWHM by more than 0.8 keV due to the cable tree can be excluded.

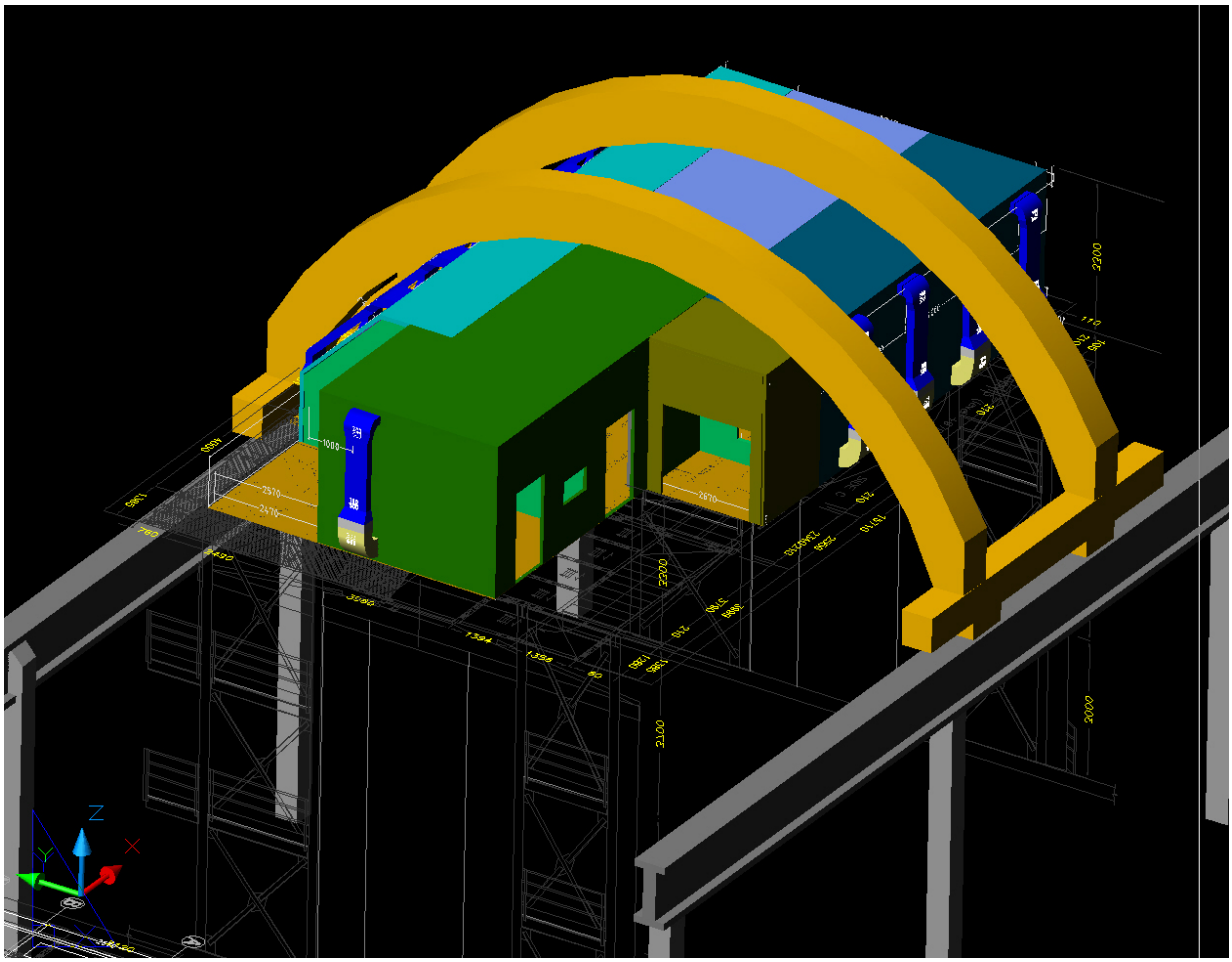

Figure 11: 3D Model of the GERDA clean room on the superstructure platform underneath the crane bow.

6 Front End electronics

Activities for the development of front end electronics concentrated on two points during the last months:

- **Development of ASIC CMOS Charge Sensitive Amplifiers (CSA)**: In November 2007 a new version of the PZ0 and PZ1 chips have been submitted to the foundry. Improvements include an increase in the number of channels per chip from one to three and further integration of external components on PZ1. The chips have been received in February 2008 and their characterization will commence soon.

- **Test of FE circuits with detector**: The test of the CSA candidate IPA4 to be adopted in GERDA Phase I with a detector in liquid nitrogen/argon has been postponed since the available detectors have been used for stability investigations. For this reason two test assembly equipped each with a crystal have been built. They are the SUB and the GERDELLA assembly. The SUB is shown in Fig. 12: A p-type detector is enclosed in a sealed vacuum container while the FE circuit under test is located outside. The entire setup is then submerged in a cryogenic liquid. Comparative tests with CSA amplifier mounted to the SUB have started and first results with the PZ0 (CSA77) gave a resolution of 2.6 (3.0) (FWHM) for 1.3 MeV ^{60}Co. The next CSA under test will be the IPA4 and PZ1.

  The second test bench GERDELLA is illustrated in Fig. 13. An n-type detector is encapsulated in a vacuum sealed special aluminum can and it is cooled down by slowly immersing it and the FE CSA in the cryogenic fluid. The detector is one from the former EUROBALL experiment. The best resolution obtained until now with the GERDELLA test bench is 5.1 keV, limited both by low frequency (LF) and HF noise coming from pick-up of glitches from switching units and boiling off of cryogenic liquid. Once the two test benches exhibit a better noise performance they will be used for cold FE CSA tests. An intense campaign of measurements is planned for the near future.

Figure 12: The SUB detector assembly.

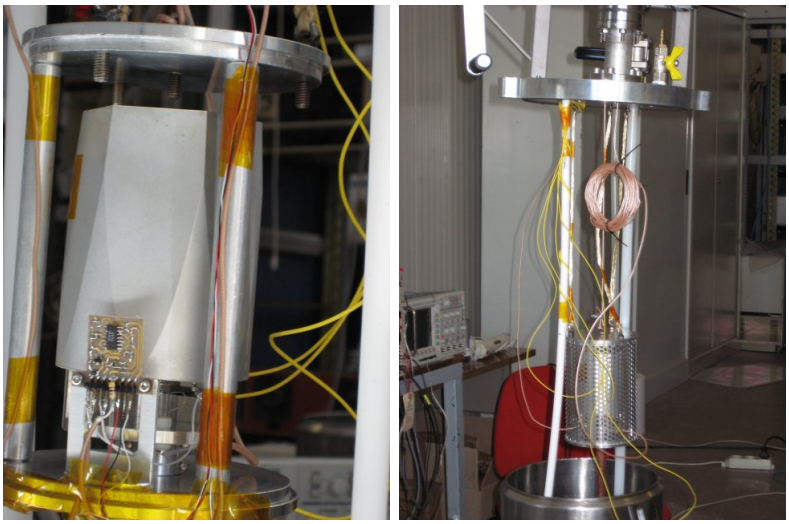

Figure 13: The IPA4 circuit connected to the EUROBALL detector and mounted in GERDELLA.

7 DAQ electronics and online software

The DAQ electronics for the readout of the diodes of phase I is ready and the setup will be tested in the LArGe facility.

During the last months the strengthened group in Padova has started to build up the slow control of the experiment based on their expertise with a similar system for the Opera experiment [1].

Gerda will be equipped with a slow control system with responsibility for:

- low and high voltage power supplies control and monitor;
- monitoring of parameters characterizing the status of the sub-systems, like temperature, pressure, detector currents, etc.;
- readout of several sub-component parameters and storage in a database for later retrieval;
- alarm handling;
- providing a graphical user interface (GUI) for sub-systems breakdown;
- producing online histograms for the relevant parameters;
- reliable remote monitoring of the whole experiment.

Its main building blocks are listed below:

- A database is the heart of the system; it stores both the slow control data and the slow control configurations. We have selected PostgreSQL [2] as relational database. Due to the possible high number of records in the data tables, the database will be splitted in two: the so-called online database where all data are stored frequently, and the historical database where older data are copied regularly after having applied some data reduction algorithms.
- The acquisition task will be performed by a pool of clients, each serving a dedicated hardware sub-component. The clients will store the acquired data in the Slow Control database.
- A supervisor process, the alarm manager, retrieves data from the database and is able to generate warnings or error messages in case of detector malfunctioning.
- The system will be completed by useful tools for the data taking, like a histogram viewer and an alarm viewer.
- Safety relevant alarms generated autonomously by some components will go directly to the LNGS safety system and to the Gerda on-call experts, while the slow control system will record the event into the database for future analysis.

Since the system is largely a copy of the Opera slow control its implementation can be done with a relatively small effort.

8 Muon veto

8.1 Plastic veto

A batch of 10 plastic scintillators with dimensions of 200×50×3 cm^3 has been assembled at Dubna and first tests have been performed at Dubna, Heidelberg, Tübingen and LNGS.

The tests showed that the concept works, but more wavelength shifting fibers and green-extended H6780-20 phototubes are desirable for improved performance. The background due to gammas inside the LNGS tunnel is lower by a factor 2 than outside. The gammas and muons give distinct signals.

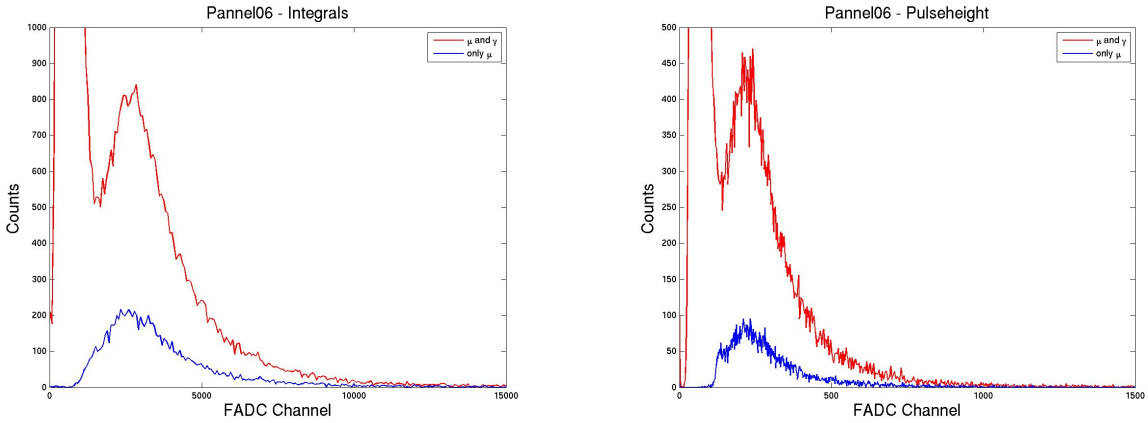

Figure 14: Response of a plastic scintillator panel to gammas and muons. The spectra have been accumulated for the integral of the FADC pulse (left) and the maximum pulse height (right).

8.2 Cherenkov veto

The preproduction assembly has been performed by building five complete PMT capsules and it revealed a few minor problems which have been solved meanwhile. Tightness around the flange is achieved by additional glueing of the PET window. Furthermore, as the actual size of the PMTs varies widely, more time is needed to fit the PMT properly into its capsule.

In parallel, work on the LED flashing and monitoring system is performed as well as on digitization.

According to recent tests the water resistance of the VM2000 foil is good enough to allow the glue to remain on the backside of this reflector foil. Presently we are investigating to use this adhesive to fix the foil directly onto the walls of the water tank and the outer wall of the cryostat. Still, the foreseen studs will be used to secure the VM2000 foil thus reducing the risk that the foil tears off the wall during fast water drainage and subsequently clogs the water pipe. The present mounting will increase safety in a double way:

- (i) the paper backing of the foil which covers the glue will be removed
- (ii) the VM2000 foil is fixed by two independent measures to the walls

A further stability test of the foils and their anchorage can be performed during the hydrostatic test of the water tank. The production of the PMT encapsulation will be finished by July 2008. They will be ready for mounting inside the water tank after its final test and during the construction of the penthouse. The plastic scintillators are planned to go onto the roof of the penthouse during the 'dirty' part of the work before establishing clean room conditions inside.

9 Monte Carlo simulations and background studies

The activity of Task Group 10, which is devoted to Monte Carlo simulations and background studies, was focused in the last six months to improve and develop the GEANT4-based framework MAGE, in collaboration with the MAJORANA Monte Carlo group. A general paper describing the structure and the functionalities of MAGE has been submitted for publication. It summarizes the status of MAGE and the four-year development performed up to now. The preprint is available on arXiv [3].
The main goal for the next few months is to perform a new full Monte Carlo campaign to estimate the total background spectrum in GERDA, taking into account the most recent information about the geometry and the material radiopurity.

9.1 Improvements in MaGe

MAGE has been modified to be compiled optionally with the GDML libraries. GDML stands for Geometry Description Markup Language and it is designed as a standard geometry exchange format among various softwares. A geometry defined in a GDML file can be used by GEANT4, or by ROOT, or be exported from a technical drawing created by CAD tools. It is now possible to read (write) MAGE geometries from (to) GDML files and use them for the simulation.
A GEANT4-based tool to debug complex geometries has also been implemented in MAGE: it allows to check if volumes placed in the geometry are overlapping with other existing volumes at the same hierarchy level or with the mother volume. Overlapping volumes can result in crashes or infinite loops during the simulation and hence should be avoided.
Many technical details of the GERDA setup have been finalized recently, or they are close to be finalized. Therefore the GERDA geometry in MAGE has been significantly updated. The most important changes are related to the geometry of the detector strings and of the cryostat.
A more realistic estimate of the dimensions of the Phase II germanium detectors has been implemented. The dimensions are decreased to those of the true-coaxial prototype detectors at MPI-Munich, namely $r_i = 5$ mm, $r_o = 37.5$ mm and height = 70 mm. The detector holder geometry and cabling are also updated to the latest design, reducing the amount

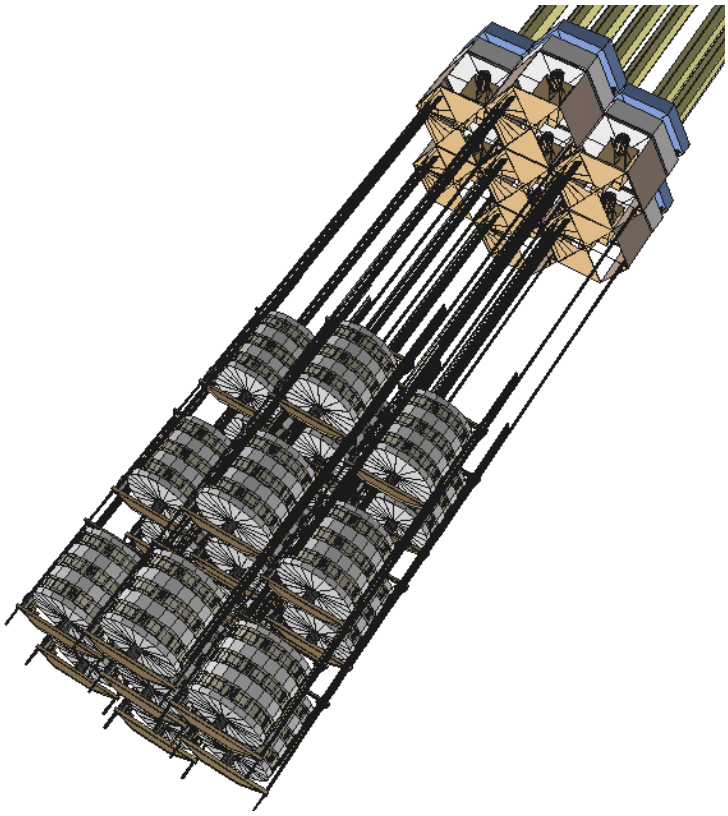

Figure 15: View of the detector array string (Phase II) as modeled in MaGe.

of material close to the detector. For the first time, a complete and realistic geometry of the whole Phase II holder and cabling above the crystal was implemented into MaGe (see Fig. 15). An update of the Phase I string in MaGe has begun.
The newly implemented model of the cryostat is shown in Fig. 16. Now, shape and parameters of the copper shield have been updated, the Makrolon layer on the inner wall of the cryostat and the Torlon pads in the insulation gap have been added.
New computing resources are accessible for the MPI-Munich group. The farm is based on Intel Xeon processors running 64-bit Linux systems. In total there are 56 3.2 GHz CPUs and 168 3.06 GHz CPUs. Approximately 10 TB of storage space is available.

9.2 Estimate of tolerable material contamination

Monte Carlo simulations have been used in order to derive the maximum tolerable radioactive contamination for specific materials or detector parts.
A full MaGe-based simulation has been performed to evaluate the maximum tolerable ^{232}Th activity in the water buffer, the stainless-steel of the cryostat and the internal copper lining. Results are summarized in Table 2. The screening results are all well below the listed values, e.g. the steel activity is typically 1 mBq/kg.

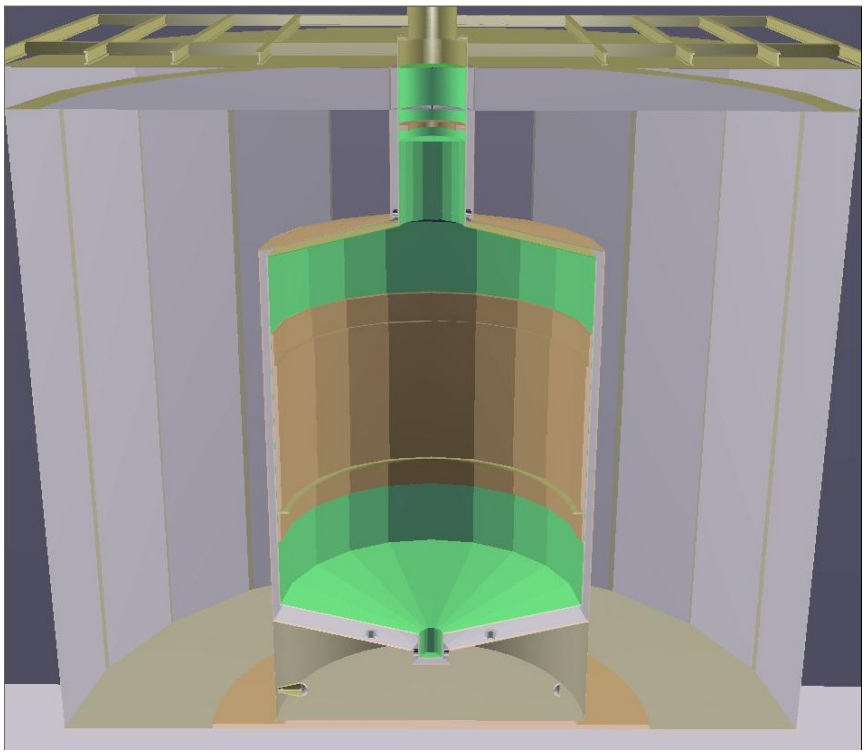

Figure 16: The cryostat inside the water tank as modeled in MaGe.

The maximum tolerable ^{222}Rn emanation rate inside the cryostat was estimated. Decays from ^{214}Bi, which is the only unstable isotope in the ^{222}Rn chain emitting γ-rays above the $Q_{\beta\beta}$-value of ^{76}Ge, have been generated uniformly distributed inside the cryogenic liquid.[3] The crystal array is assumed to be composed by 24 detectors, 15 segmented and

[3] It is unclear whether this assumption is correct. On one hand it is conservative, because it is likely that the activity is larger close to the walls of the cryostat, where ^{222}Rn is mostly emanated. On the other hand convection or electrical fields might transport the Rn close to the detectors.

Material	No cut	Crystal anti-coincidence	Segment anti-coincidence
Water	42 mBq/kg	74 mBq/kg	105 mBq/kg
Stainless steel	26 mBq/kg	46 mBq/kg	64 mBq/kg
Copper lining	110 μBq/kg	190 μBq/kg	270 μBq/kg

Table 2: Allowable ^{228}Th specific activity for individual background contributions below 10^{-4} cts/(keV·kg·y), with different conditions of background rejection. The crystal array is assumed to be composed by 24 detectors, 15 segmented and 9 unsegmented.

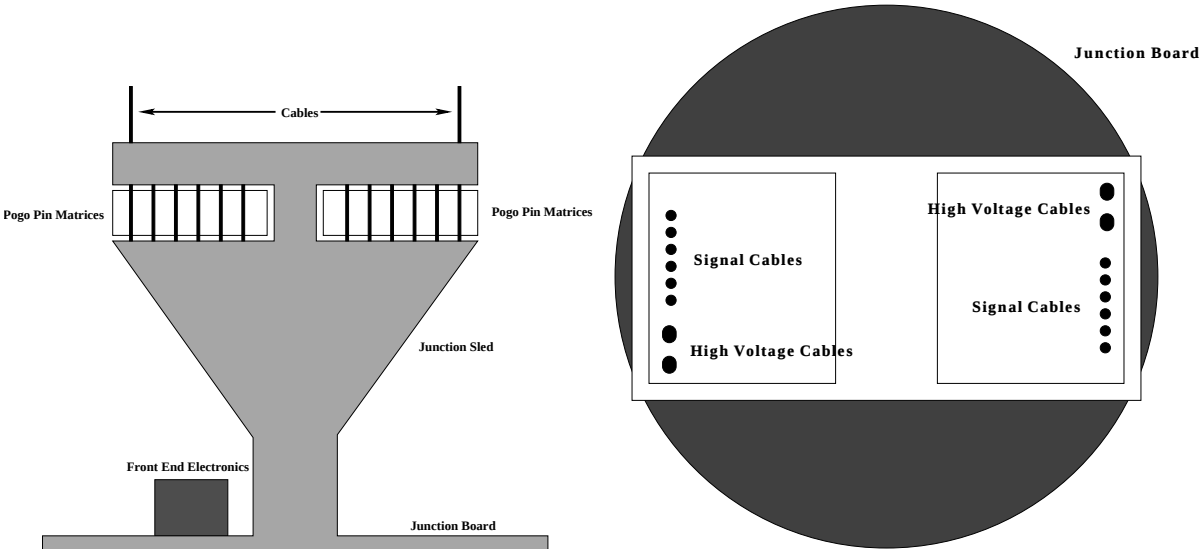

Figure 17: Schematic drawing of the junction sledge in side (left) and top view (right) as it was used in the estimate of the background contribution of connectors and cables. The design has been revised afterwards.

9 unsegmented. The maximum allowable ^{222}Rn total emanation rate for a background contribution below 10^{-4} cts/(keV·kg·y) is found to be between 8 mBq (without any cut for background suppression) and 14 mBq (with segment anti-coincidence). Results obtained with MaGe have been cross-checked using an independent stand-alone Monte Carlo simulation developed by the Russian groups of Gerda.

Also the background contribution of the cable connectors (pogo pins) and the cables connecting the detectors to the cleanroom was estimated using MaGe. The simulated setup consists of seven detector strings, each containing three 18-fold segmented detectors. The pogo pins are located 36 cm above the upside of the uppermost detectors, inside the pogo pins matrix. Each string has 120 pogo pins. The lower ends of the cables are located 38.5 cm above the uppermost detectors. Twelve signal cables and four high voltage cables have been simulated. A schematic drawing of the interim design as used in the simulation is shown in Fig. 17. The background contribution due to ^{228}Th in the cable connectors was evaluated using the crystal anti-coincidence and segment anti-coincidence cuts: the allowed ^{228}Th contamination resulting in a background index of 10^{-4} cts/(keV·kg·y) is about 17 mBq/kg and 60 mBq/kg for crystal anti-coincidence and segment anti-coincidence, respectively. The background contribution of the cables due to ^{228}Th resulting in a background index of 10^{-4} cts/(keV·kg·y) is about 1.9 mBq/kg and 8.0 mBq/kg using crystal anti-coincidence and segment anti-coincidence cut, respectively.

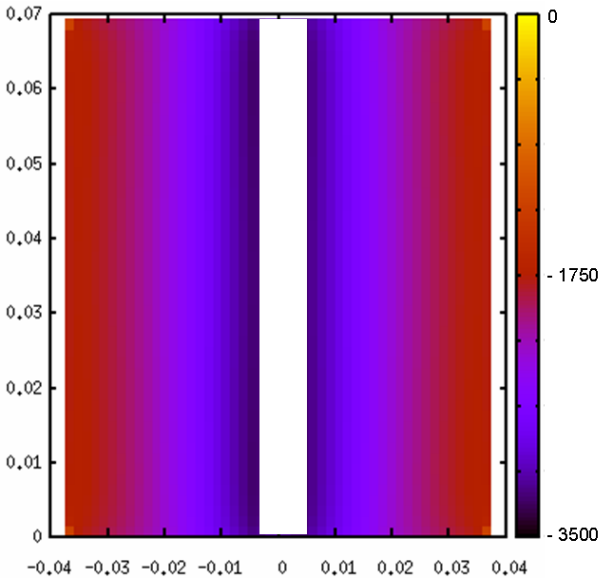

Figure 18: Electric potential calculated using the "method of successive over-relaxation" for a true-coaxial prototype detector for Phase II ($r_i = 5$ mm, $r_o = 37.5$ mm and height = 70 mm). A voltage of -3500 V is applied at the core. No space charge is assumed.

9.3 Pulse shape analysis

The pulse shape simulation is under development: the main aim is to provide a full-chain simulation of the data that will be available in GERDA, to be used to tune and benchmark the reconstruction and data analysis algorithms. The collaboration with the MAJORANA Monte Carlo group is going on also in this sector, with the joint development of common interfaces, called MGDO (Majorana-GERDA Data Object), to be used for data analysis and pulse shape simulation.
The important steps toward a full pulse shape simulation are:

- simulation of energy deposition in the detectors;
- calculation of the electric and weighting fields;
- drift of the charge carriers through the crystal;
- model of the preamplifier and DAQ properties.

The simulation of the energy deposition in the crystal is done using the MAGE framework. A framework for the pulse shape simulation including interface classes to MAGE was set up. The electric field was calculated using the "method of successive over-relaxation" and first results are available (see Fig. 18). The implementation of the charge carrier drift in the crystal is ongoing.

10 Material screening

10.1 Radon measurements

10.1.1 Emanation measurements of small components

Material screening by means of the ^{222}Rn emanation technique is continuously ongoing. Samples tested in the last months were

- WTA valve: The cast-housing was identified as source of the previously reported high emanation rate of $\sim$ 2mBq. After etching the value was reduced by a factor of 10. Further investigations are ongoing.
- HV feed-through from Padova: An upper limit of 50 μBq/piece was found.
- solder: For some tens of grams < 40 μBq could be derived.
- induction sensors: They showed a rate of (16 ± 3) μBq/piece.
- cables: A coaxial signal cable (Habia, Teflon coated) and a HV (Teledyne Reynolds, Teflon coated) cable emanate with (0.50 ± 0.14) μBq/m and (1.8 ± 0.5) μBq/m, respectively.
- TIG welding: 12 mm thick samples of 2.5 m total weld length gave (0.36 ± 0.04) mBq/m. For the total cryostat weld length of $\sim$ 100 m this corresponds to $\sim$ 18 mBq for the inner surfaces of the welds. After pickling and passivation a fraction of the samples the rate was reduced to < 0.04 mBq/m ($\sim$ 2 mBq for the cryostat welds) and after electro-polishing a different fraction we found (0.10 ± 0.04) mBq/m. The higher value of the latter might be due to re-contamination after the polishing.

10.1.2 Emanation measurements of the cryostat

After the inner vessel of the cryostat was welded and pickled a first ^{222}Rn emanation test was performed. The inner vessel was closed with a carbon steel flange sealed by a Helicoflex gasket. In order to remove residual air the vessel was evacuated and filled twice with ^{222}Rn-free nitrogen. The ^{222}Rn purification was done using the activated carbon traps of the Mobile Radon Extraction Unit (MoREx). Then the vessel was pressurized up to 1.6 barg and closed to accumulate the emanated ^{222}Rn. After six days, samples of 23 m^3 (STP) and 45 m^3 (STP) were extracted and saturation emanation rates of (16.9$\pm$1.6) mBq and (29.8$\pm$2.4) mBq, respectively, were measured. Since the results do not agree within the statistical uncertainties, systematic effects must be present. In the extraction, gas is taken from the top. Therefore a non-homogeneous distribution of radon inside the vessel could explain the difference.
Since the second value was quite large, another pickling was performed and another measurement prepared. Now, only a small overpressure of 0.4 bar was used during the ^{222}Rn accumulation time and just before extraction the vessel was pressurized to 1.8 barg with

(cold) ^{222}Rn-free nitrogen, i.e. a "mixing step" was introduced. The following two extractions gave consistent results of (13.6 ± 2.5) mBq and (13.7 ± 2.8) mBq.
Previous measurements of pure stainless steel samples gave 5 μBq/m^2 corresponding to only 0.4 mBq for the cryostat's surface area. Emanations from welds are therefore expected to dominate. The obtained result is higher than the extrapolation from the emanation of the pickled welding samples ($\sim$ 2 mBq). However, large-scale pickling of the cryostat might not be as effective as small-scale pickling in the laboratory and some dust and remnants from markers and tape are still present in the cryostat.

10.1.3 Behavior of radon in liquid nitrogen

For the GERDA experiment the behavior of ^{222}Rn and its daughters in cryogenic liquids (LN_2, LAr) is of great importance. The electric field created by the high voltage (HV) applied to the detectors and possible convection movements of the cryo-liquid can lead to the migration of radioactive isotopes and their possible accumulation close to the diodes. Decaying there they would significantly contribute to the background of the experiment. A special programm to carefully investigate that problem has been established. For measurements an experimental setup consisting of a 32-liter dewar, an evaporator, a scintillation chamber (to measure the Rn concentration in gases), a gas flow meter and a data acquisition system was used.

First the radon partition coefficient between the liquid and gas phase of nitrogen was measured. After dissolving ^{222}Rn in LN_2 (contained in the 32-l dewar) the concentrations in the boil-off and in the gas evaporated directly from the liquid phase were investigated. For the free evaporation we got a ratio of 16.3 ± 1.7 (liquid/gas, concentrations determined always at STP). Further tests showed that this factor depends on the evaporation rate: the faster the evaporation is, the higher is the ^{222}Rn content in the boil-off N_2.

To investigate the behavior of radon in the liquid nitrogen, stainless steel discs (25 mm in diamater) were used. The ^{222}Rn decay products (mainly polonium isotopes) plate-out on their surfaces and can then be counted using an alpha spectrometer. In this way, after dissolving radon in the liquid nitrogen, it was possible to monitor its concentrations at different positions in the dewar and also under various conditions like: exposure time (from 3 h to several days), electric field strength (HV applied to the disc), gaseous or liquid environment. Obtained results show that deposited Po isotopes were not in radioactive equilibrium even for exposure longer than 3 hours. In addition a rapid increase of the number of Po atoms deposited on the steel surface was observed after applying HV to the discs (up to 2.5 kV, see Fig. 19). For +2 kV the activity of accumulated ^{214}Po was about 12 times higher than that obtained without HV. This effect was even stronger for negative voltages: at -2 kV the mentioned above ratio was about 36. Measured Po activities as a function of the "storage" time (time elapsed since ^{222}Rn dissolving, no mixing in between) indicate that some kind of ^{222}Rn-'cloud' has formed close to the steel discs.

As it can be seen in Fig. 20 the amount of Po accumulated on a disc placed always in the

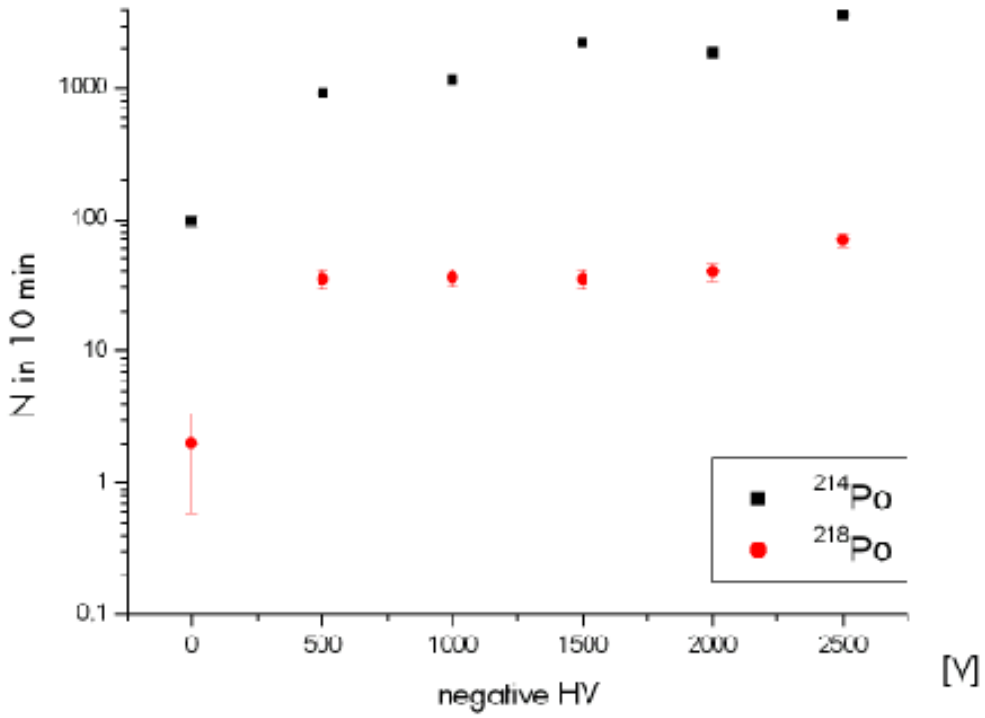

Figure 19: Activity of ^{214}Po and ^{218}Po plated-out on a disc on negative high voltage.

same position in the dewar rises with the time elapsed since the moment of ^{222}Rn dissolving (interpreted as a slow cloud formation). After mixing of the LN_2 (last measurement point) the cloud disappears and the amount of plated-out polonium drops down to the initial value.

The discovered effect may suggest that ^{222}Rn atoms 'feel' an electric field what may cause their local accumulations. This phenomena may be problematic for the GERDA experiment and needs good understanding. Next tests with a germanium disc and LAr are planned.

10.2 Gamma ray screening

In the last months the main focus in gamma ray screening was put on electronics components, parts for the Ge-diodes suspension system, and for LArGe. Samples were measured in the Germanium spectrometers of IRMM/Hades, Gran Sasso and Baksan. The results for the electronics components are summarized in Table 3. As usually they are relatively high in U/Th/K (activities in the range of Bq/kg). As a result of the screening measurements some of the components for the LArGe setup had to be replaced.

Table 4 summarizes the results for further samples measured during the last 6 months. Another batch of stainless steel plates with ^{226}Ra/^{228}Th activities below 1 mBq/kg was identified, which can be used for cable chains. Also stainless steel ropes for the suspension

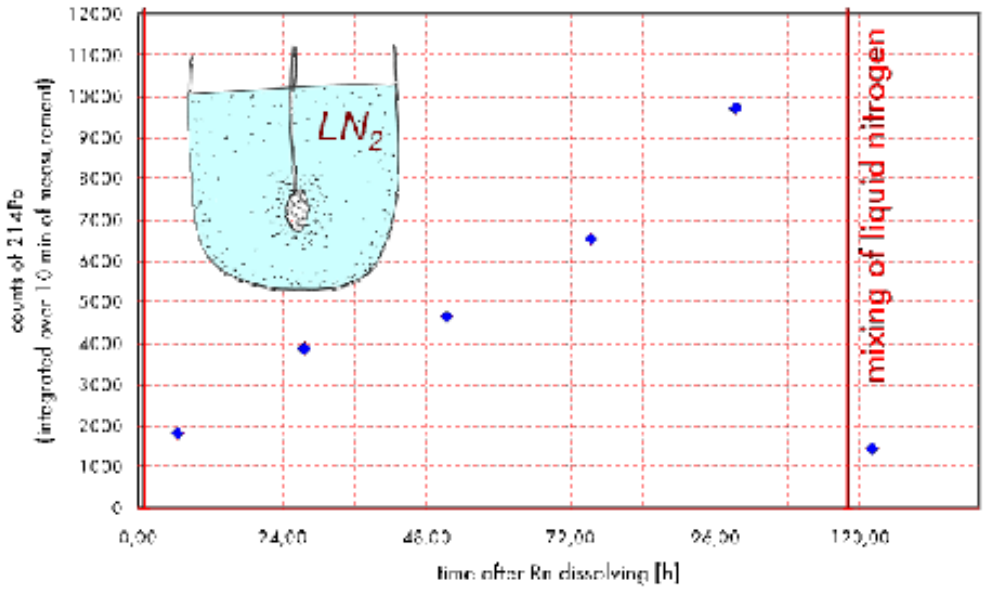

Figure 20: ^{214}Po activity as a function of the time elapsed since radon dissolving in the dewar. -2 kV applied to the discs.

system were measured. Since initial results were very high a cleaning procedure by ultrasonic soap cleaning and subsequent 2-propanol rinsing was performed. All contaminants except ^{60}Co (which is likely a bulk contamination) were reduced significantly (factor 400 for ^{40}K).

10.3 Low-level instrumentation

10.3.1 Gas counting setup

During the installation phase of GERDA on-site ^{222}Rn-measurements with proportional counters will become more important. Therefore, a dedicated sample preparation and ^{222}Rn-counting system close to the GERDA site is required. We plan to re-use the ultra-low background counting setup of the former GALLEX/GNO experiments. For this purpose a gas handling and counter filling line was built in Heidelberg. Commissioning of the line will start in April and after a short phase of thorough testing it is supposed to move to Gran Sasso in summer 2008. It features not only the required equipment for ^{222}Rn-counting, but also for the analysis of other radioactive noble gases like ^{39}Ar, ^{85}Kr and ^{133}Xe, which might be interesting for further applications within GERDA and beyond. Also a dedicated VME-based DAQ system was developed in Heidelberg and is ready to be used at Gran Sasso.

Sample	specific activities [Bq/kg]				
	^{228}Ra	^{228}Th	^{238}U	^{226}Ra	^{40}K
Suhner HV feedthr.	—	0.23 ± 0.02		0.51 ± 0.04	35.7 ± 0.4
Suhner signal feedthr.	—	0.04 ± 0.01		0.07 ± 0.02	6.2 ± 0.2
Capacitors 8200 pF	1.3 ± 0.1	1.0 ± 0.1	0.4 ± 0.1	$5.2 \pm 0.3^{*)}$ $5.7 \pm 0.4^{**)}$	2.5 ± 0.2
Capacitors 4700 pF	1.3 ± 0.1	0.9 ± 0.1	2.2 ± 0.3	$11.6 \pm 0.6^{*)}$ $14.1 \pm 0.9^{**)}$	0.8 ± 0.2
Resistors 470 kΩ	0.13 ± 0.03	0.20 ± 0.02	0.4 ± 0.2	$0.28 \pm 0.03^{*)}$ $0.6 \pm 0.1^{**)}$	0.2 ± 0.1

*) From ^{222}Rn-daughters / Some ^{222}Rn may have escaped. **) From the 186 keV line of ^{226}Ra.

Table 3: Summary of gamma ray screening results of electronics components for GERDA.

10.3.2 Germanium spectrometers

An new ultra-low background HPGe detector (GATOR) which will be shared between the XENON and the GERDA experiments has been installed in the Gran Sasso underground laboratory. It is a 2.2 kg crystal with 100 % relative efficiency and a shield made out of 5 cm copper and 20 cm lead. The whole setup is in an air tight box which is continuously flushed with nitrogen to remove atmospheric radon. The first background spectrum shows a rate significantly less than 1 count/(kg·keV·day) above 40 keV. Since GATOR features also a large sample chamber it will be a valuable new spectrometer for ultra-sensitive measurements.

After the end of the renovation work in the Heidelberg shallow depth underground laboratory the re-commissioning of the spectrometers has started. Bruno and Corrado are running again, whereas Dario does not work properly. Meanwhile it was removed from its shield to check the reason for its failure. Also another detector, Adam, which was not operated for several years, is now running again. Adam is a bore-hole detector surrounded by a lead shield and muon veto proportional counters. First background measurements and tests of the veto system will start soon.

Sample	specific activities [mBq/kg]				
	^{228}Th	^{238}U	^{226}Ra	^{40}K	^{60}Co
Stainless steel plates	0.6 ± 0.2	—	$0.8 \pm 0.3^{*)}$ $< 3.7^{**)}$	1.2 ± 0.4	13 ± 1
Stainless steel cables before cleaning	13.4 ± 1.5	—	13.2 ± 1.6	3600 ± 200	172 ± 9
Stainless steel cables after cleaning	2.1 ± 1.0	—	3.1 ± 1.5	< 9	200 ± 12
Copper screws	< 1	—	< 1	< 7	< 0.5
VM2000 foil with glue	< 1.2	< 39	< 1.6	140 ± 10	—
PMT bases	14 ± 1	650 ± 80	< 5.9	340 ± 20	—

*) From ^{222}Rn-daughters / Some ^{222}Rn may have escaped. **) From the 186 keV line of ^{226}Ra.

Table 4: Summary of gamma ray screening results of different components foreseen to be used for the GERDA detector suspension system and for LArGe.

References

[1] A. Bergnoli et al., *T*he OPERA spectrometer slow control system, IEEE Trans.Nucl.Sci. 55 (2008) 349-355.

[2] The PostgreSQL database, `http://www.postgresql.org/`.

[3] Y.D. Chan et al., *MaGe - a Geant4-based Monte Carlo framework for low-background experiments* , submitted to IEEE Trans. Nucl. Scie., preprint arXiv:0802.0860v1 (2008)